Structurally modulated codelivery of siRNA and Argonaute 2 for enhanced RNA interference

Jiahe Li[a,b], Connie Wu[a,b], Wade Wang[a,c], Yanpu He[a,b], Elad Elkayam[d,e], Leemor Joshua-Tor[d,e], and Paula T. Hammond[a,b,1]

[a]Koch Institute for Integrative Cancer Research, Massachusetts Institute of Technology, Cambridge, MA 02139; [b]Department of Chemical Engineering, Massachusetts Institute of Technology, Cambridge, MA 02139; [c]Department of Chemistry, Massachusetts Institute of Technology, Cambridge, MA 02139; [d]W. M. Keck Structural Biology Laboratory, Cold Spring Harbor Laboratory, Cold Spring Harbor, NY 11724; and [e]Howard Hughes Medical Institute, Cold Spring Harbor Laboratory, Cold Spring Harbor, NY 11724

Edited by Sang Yup Lee, Korea Advanced Institute of Science and Technology, Daejeon, Republic of Korea, and approved January 16, 2018 (received for review November 9, 2017)

Small interfering RNA (siRNA) represents a promising class of inhibitors in both fundamental research and the clinic. Numerous delivery vehicles have been developed to facilitate siRNA delivery. Nevertheless, achieving highly potent RNA interference (RNAi) toward clinical translation requires efficient formation of RNA-induced gene-silencing complex (RISC) in the cytoplasm. Here we coencapsulate siRNA and the central RNAi effector protein Argonaute 2 (Ago2) via different delivery carriers as a platform to augment RNAi. The physical clustering between siRNA and Ago2 is found to be indispensable for enhanced RNAi. Moreover, by utilizing polyamines bearing the same backbone but distinct cationic side-group arrangements of ethylene diamine repeats as the delivery vehicles, we find that the molecular structure of these polyamines modulates the degree of siRNA/Ago2-mediated improvement of RNAi. We apply this strategy to silence the oncogene STAT3 and significantly prolong survival in mice challenged with melanoma. Our findings suggest a paradigm for RNAi via the synergistic coassembly of RNA with helper proteins.

siRNA | RNA interference | Argonaute | polyamines | gene delivery

RNA interference (RNAi) has recently emerged as a potent antisense oligonucleotide therapeutic strategy for gene silencing (1). Delivery of short, double-stranded RNAs—namely, small interfering RNAs (siRNAs), which are 19–23 nucleotides in length and contain a passenger strand and its complementary strand—coopts a ubiquitous pathway to degrade target gene mRNA and suppress its expression with high specificity. Consequently, siRNAs can potentially target undruggable gene products and allow for rapid validation of drug inhibitors. Despite powerful genome-editing technologies such as clustered regularly interspaced short palindromic repeats (CRISPR), interventions at the mRNA level are still highly desirable for the majority of therapeutic applications that require temporary gene knockdown, such as regulation and alleviation of inflammatory responses (e.g., myocardial infarction) or cases in which off-targeting at a genomic level could lead to permanent deleterious mutations (2–5). In the past decades, numerous siRNA carriers and chemical modifications of the RNA backbone have been developed to protect siRNA from degradation, enable uptake by cells, improve encapsulation, or facilitate endosomal escape of siRNA (6–9). Nevertheless, achieving high RNAi efficiency remains challenging for the clinical translation of siRNA therapeutics.

In this study, we explored a different route to enhance RNAi by physically clustering duplex siRNA with the central RNAi effector protein Argonaute 2 (Ago2) via cationic lipids or structurally defined synthetic polypeptides, which was inspired from several lines of evidence: (*i*) Microvesicles secreted from cultured cancer cells or activated platelets are found to contain microRNA (miRNA)/Ago2 complexes that serve to stabilize the small RNAs and mediate potent silencing of the target mRNA in recipient cells (10, 11). (*ii*) An in vivo study discovered that the inhibitory effects on mRNA and protein levels are largely determined by the abundance of Ago2-bound siRNA, rather than the total amount of siRNA (free and Ago2-bound siRNAs). Consequently, siRNA-mediated in vivo silencing activity and duration are based on the number of Ago2-siRNA complexes and the complex stability over time (12). (*iii*) Biochemists have successfully loaded short, single-stranded small interference RNA (ss-siRNA) or duplex siRNA containing guide and passenger RNAs into Ago2 in vitro for gene-silencing assays (13–16). (*iv*) More recently, an ss-siRNA/Ago2 complex system was used to silence mRNAs in *Cryptosporidium*, which lacks key components of RNAi, for interrogating parasite–host interactions (17). (*v*) The availability of recombinant RNA-free human Ago2 has accelerated the efficiency of loading desired siRNA for fundamental research (13).

To demonstrate that enhanced gene silencing can be achieved by delivery of siRNA/Ago2 complexes, we first used commercial polymer or lipid-based transfection reagents designed for in vitro use to examine the impact of preassembly of the complex versus siRNA alone. We then synthesized a series of polyamines bearing the same polyaspartamide backbone but with differing lengths of side-chain amine structures and accompanying charge densities and arrangements. These polyamines have been primarily used for the protection, cellular uptake, and sustained delivery of DNA and mRNA, with high transfection efficiency, biocompatibility, and biodegradability in vitro and in vivo (18–20). In this work, however, we repurposed these structurally

Significance

Small interfering RNA (siRNA) has great potential to specifically target undruggable genes in many diseases. Despite its great promise, few siRNAs have been clinically approved due to limited therapeutic efficacy. We propose that one major barrier to RNA interference (RNAi)-based therapy is that the siRNA must form a bound complex with a "scissor" protein, Argonaute 2 (Ago2), after it is released in the cytoplasm. We take the approach of preassembling the duplex siRNA with Ago2 protein, and then packaging the complex with commercial transfection reagents or structurally defined polycations that specifically enhance the clustering of siRNA with Ago2. This unique approach augments gene silencing in cell lines and a melanoma mouse model, providing a potential translatable platform for RNAi therapies.

Author contributions: J.L. designed research; J.L., C.W., W.W., and Y.H. performed research; W.W., E.E., and L.J.-T. contributed new reagents/analytic tools; J.L., C.W., Y.H., E.E., L.J.-T., and P.T.H. analyzed data; and J.L., C.W., and P.T.H. wrote the paper.

Conflict of interest statement: A provisional US patent application (62/505,430) on this work has been filed.

This article is a PNAS Direct Submission.

[1]To whom correspondence should be addressed. Email: hammond@mit.edu.

This article contains supporting information online at www.pnas.org/lookup/suppl/doi:10.1073/pnas.1719565115/-/DCSupplemental.

Published online February 5, 2018.

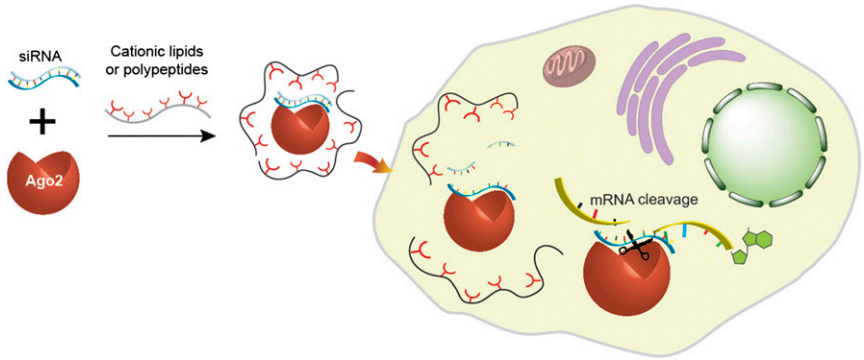

Fig. 1. A schematic of the codelivery of siRNA/Ago2 complex into cells. The complex is encapsulated by cationic lipids or synthetic polyamines. Following intracellular delivery, the passenger strand of duplex siRNA gets cleaved and dissociates from Ago2 during the assembly of RISC (40, 42), leaving the antisense-strand-loaded Ago2 available for recognition and cleavage of target mRNA over a sustained period of time.

defined polyamines to coassemble siRNA/Ago2 complexes and elucidated key structure–activity relationships for enhanced RNAi efficiency (Fig. 1). Notably, in contrast to a previously described "odd–even" effect on DNA and mRNA delivery (18, 21), we unveiled different rules associated with these unique features that govern the coassembly and resulting gene-silencing efficiency of siRNA/Ago2 complexes through biophysical and polymer chemistry approaches. Finally, to demonstrate the therapeutic potential of our system, as a proof-of-concept we chose to target signal transducer and activator of transcription 3 (STAT3), whose overexpression has been linked to tumor progression, drug resistance, promotion of cancer stem cells, and immune evasion in different cancers (22–24). To this end, we explored whether codelivering anti-STAT3 siRNA with Ago2

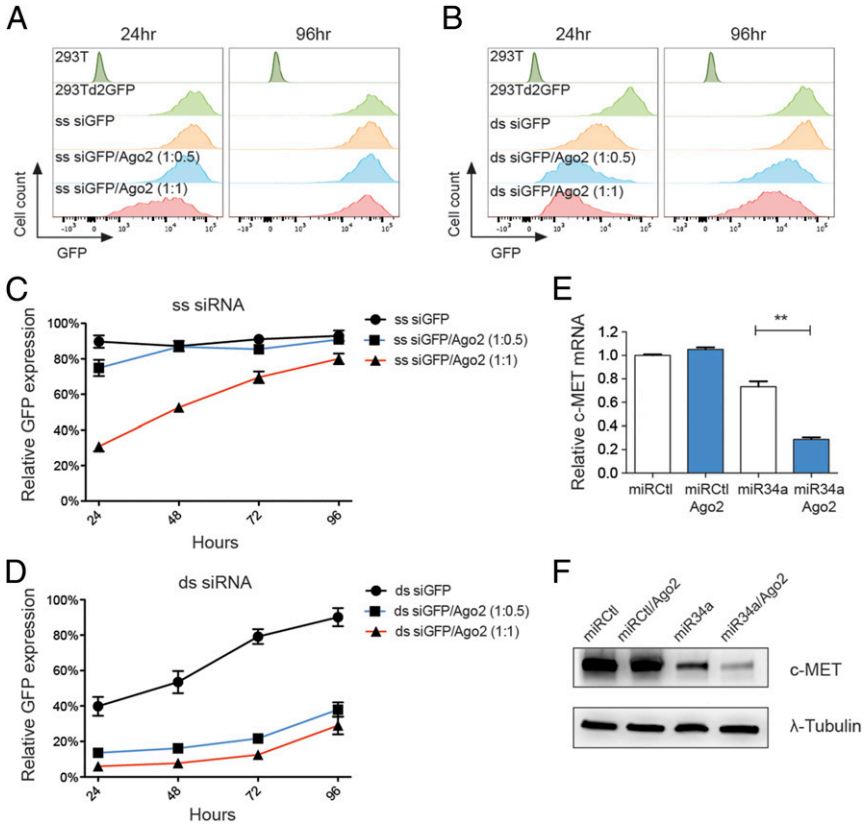

Fig. 2. ds siRNA or miRNA mimics loaded with Ago2 elicit superior gene silencing. ss siGFP (25 nM), ds siGFP (25 nM), or siGFP (25 nM)/Ago2 at two different molar ratios (1:0.5 and 1:1 RNA:Ago2) were transfected using TransIT-X2 into 293Td2GFP cells. Mean fluorescence intensity of GFP expression was quantified via flow cytometry. Representative histograms of GFP expression at 24- and 96-h posttransfection are shown for (*A*) ss siGFP and (*B*) ds siGFP. Quantification of GFP expression normalized to that of nontransfected 293Td2GFP over the course of 96 h after transfection of (*C*) ss siGFP or ss siGFP/Ago2; (*D*) ds siGFP or ds siGFP/Ago2. In addition to targeting GFP, 25 nM miR34a mimics were transfected along with Ago2 at a 1:1 molar ratio using TransIT-X2. A corresponding scrambled sequence (miRCtl) was used as a negative control. Down-regulation of a miR34a target, c-MET, was confirmed by (*E*) quantitative PCR via normalization to β-actin mRNA and (*F*) Western blotting. Representative images of two independent experiments are shown. λ-Tubulin served as an internal loading control. Data for GFP silencing and qPCR are represented as the mean ± SEM ($n = 3$); $^{**}P < 0.01$.

can enhance the therapeutic efficacy of RNAi in a well-established mouse melanoma model.

Results

Double-Stranded siRNA/Ago2 Complex Is More Potent than Single-Stranded siRNA/Ago2. We genetically modified human 293T cells to stably express a destabilized version of green fluorescence protein (d2GFP) with a short half-life relative to enhanced GFP, which allows for fast readout of GFP silencing at the mRNA level (25). Meanwhile, recombinant RNA-free human Ago2 protein was produced from SF9 insect cells and purified to homogeneity using a well-established protocol (*SI Appendix*, Fig. S1*A*) (13). Next, we asked whether transfection of single-stranded anti-GFP siRNA (ss siGFP)/Ago2 complexes is more potent than ss siGFP alone in knocking down GFP expression via commercial transfection reagents. Delivery of ss siGFP with the commercial transfection agent TransIT-X2 led to little to no silencing (Fig. 2 *A* and *C*). On the other hand, transfection of ss siGFP and Ago2 complexes using TransIT-X2 significantly enhanced GFP silencing compared with the corresponding ss siRNA alone in 293T cells (Fig. 2 *A* and *C*). However, since the majority of existing siRNA-based therapeutics employ double-stranded siRNA (ds siRNA), we further tested the preassembly of ds siRNA and Ago2. It was found that ds siGFP/Ago2 induced greater reduction of GFP expression than ds siGFP alone or ss siGFP/Ago2 (Fig. 2 *B* and *D*). On the contrary, anti-luciferase siRNA (ss siLuc and ds siLuc) alone or along with Ago2 failed to silence GFP expression, ruling out the possibility of nonspecific gene knockdown due to cotransfection of Ago2 protein (*SI Appendix*, Fig. S1 *B* and *C*). We deduce that the relative low efficacy of ss siGFP alone or codelivered with Ago2 may result from lower stability of ss siRNA in the cytoplasm relative to ds RNA, leading to reduced formation of cytoplasmic RNA-induced silencing complex (RISC) (26).

In addition to targeting the internal coding sequence of genes via siRNA, we also explored preassembly of Ago2 with miRNA mimics, which represent another class of RNAi-based therapeutics. To this end, we first inserted miR34a-binding sites into the 3′ untranslated region of GFP to examine gene silencing mediated by the tumor suppressor miR34a (*SI Appendix*, Fig. S2*A*) (25). Delivery of ds miR34a mimics along with Ago2 significantly reduced GFP expression compared with miR34a mimics alone. Notably, at 96-h posttransfection, the GFP silencing from transfection of miR34a had nearly disappeared, while sustained silencing was still detectable in the cells transfected with miR34a/Ago2 complexes (*SI Appendix*, Fig. S2*B*). In contract, a scramble control miRNA mimic did not result in GFP knockdown regardless of cotransfection of Ago2 protein (*SI Appendix*, Fig. S2*C*). Furthermore, we confirmed that miR34a/Ago2 complexes were able to silence oncogenes, c-MET and CDK4, endogenous targets of miR34a, in OVCAR8 ovarian cancer cells (Fig. 2 *E* and *F* and *SI Appendix*, Fig. S2*D*). Therefore, preassembly of ds siRNA or miRNA mimics along with Ago2 represents a promising strategy to improve the potency of RNAi, which targets either coding or noncoding sequences.

In addition to TransIT-X2, we further confirmed that a lipid-based siRNA transfection reagent, Lipofectamine RNAiMAX, was able to successfully deliver ds siGFP/Ago2 complexes with enhanced RNAi over ds siGFP alone in 293Td2GFP cells (*SI Appendix*, Fig. S3*A*). Nevertheless, a third lipid-based commercial siRNA transfection reagent, Stemfect, failed to enhance GFP silencing via codelivery of ds siGFP/Ago2 (*SI Appendix*, Fig. S3*B*). In general, there are clear indications that the efficacy of the coassembled structures is strongly dependent on the type of agent used for transfection.

The Polyamine Side-Chain Structure Modulates the Activity of siRNA/Ago2 Complexes. To define the rules that govern the coassembly and resulting gene-silencing efficiency, we utilized a series of structurally defined cationic polypeptides for the preassembly of ds siRNA/Ago2, which will be referred to as siRNA/Ago2 for the rest of this study. These polypeptides were derived using *N*-carboxyanhydride polymerization of L-benzyl aspartate, followed by exhaustive amination of the side chain with various *N*-amine substituents bearing one to four aminoethylene repeats in the side chain (Fig. 3*A* and *SI Appendix*, Fig. S4). Therefore, keeping the same backbone while using distinct side-chain structures enables in-depth characterization of synthetic gene carrier-assisted assembly and delivery of siRNA/Ago2 complexes. Moreover, these polypeptides have demonstrated superior transfection efficacy for mRNA and DNA delivery with minimal cytotoxicity in vitro and in vivo (20, 27–29).

As shown in Fig. 3 *B–D*, at an N/P ratio of 20:1 (number of protonatable amines in the polyamine relative to number of phosphates in siRNA), preassembly of siGFP/Ago2 using the polyamine series as delivery agents resulted in enhanced GFP silencing in 293Td2GFP cells compared with siGFP alone, whereas ss siLuc and ds siLuc alone or with Ago2 failed to knock down GFP expression irrespective of the polyamines under the study (*SI Appendix*, Fig. S5). Interestingly, we observed that the degree of GFP silencing in siGFP/Ago2-transfected cells was proportional to the number of amine groups on the polyamine side chain, even though the N/P ratio was kept the same across all four polyamine carriers. In addition, enhanced gene knockdown was observed by titrating concentrations of siGFP or siGFP/Ago2 from 50 to 200 nM in 293Td2GFP cells (*SI Appendix*, Fig. S6). We reasoned that the cationic charge density on the polyamine side chain is associated with the number of amine groups and degree of protonation at a given pH. Additionally, the degree of protonation is affected by the spacing between two neighboring amine groups, as protonation of neighboring amines on the 1,2-diaminoethane moiety (-NH2CH2CH2NH2-) is thermodynamically unfavorable due to electrostatic repulsion (18, 21). Consequently, at neutral pH, when gene silencing occurs in the cytoplasm, the charge unit on the polyamine side chain can be estimated as shown in Fig. 3*A*, which was found to be positively correlated with the increase in GFP silencing via preassembly of siGFP/Ago2. Such speculation can be corroborated by measurements of the sizes and zeta potentials of siRNA and siRNA/Ago2 complexed with polyamines, where increases in surface charge and condensation ability were observed from N1 (EDA) to N4 (TEP) under physiological conditions (*SI Appendix*, Fig. S7). Moreover, we found that at N/P 20, siRNA and siRNA/Ago2 did not induce cytotoxicity in immortalized fibroblast cells, which make up the majority of cell types found in many tissues, nor did the inclusion of Ago2 affect cell proliferation compared with siRNA transfection alone (*SI Appendix*, Fig. S8).

To further confirm whether protonated amine groups on the side chain play a role in modulating siRNA/Ago2 activity, we introduced an additional methylene group on the side chain of N2 (DET) to generate a side chain with 1,3-diaminopropylene ($-NHCH_2CH_2CH_2NH_2$), referred to as N2 (DPT) in this study. According to a previous finding, increased spacing between two protonatable amines in propylene compared with in ethylene repeat units reduces charge repulsion when both amines are protonated (30). Consequently, N2 (DPT) exhibits a higher degree of protonation (~88%) at pH 7.4, compared with N2 (DET), with nearly half the side-chain amines protonated based on potentiometric titration. Interestingly, as shown in Fig. 3*E*, N2 (DPT) enabled stronger GFP silencing than N2 (DET) when cotransfecting siGFP/Ago2, whereas siRNA against luciferase failed to silence GFP expression with Ago2 and N2 (DPT).

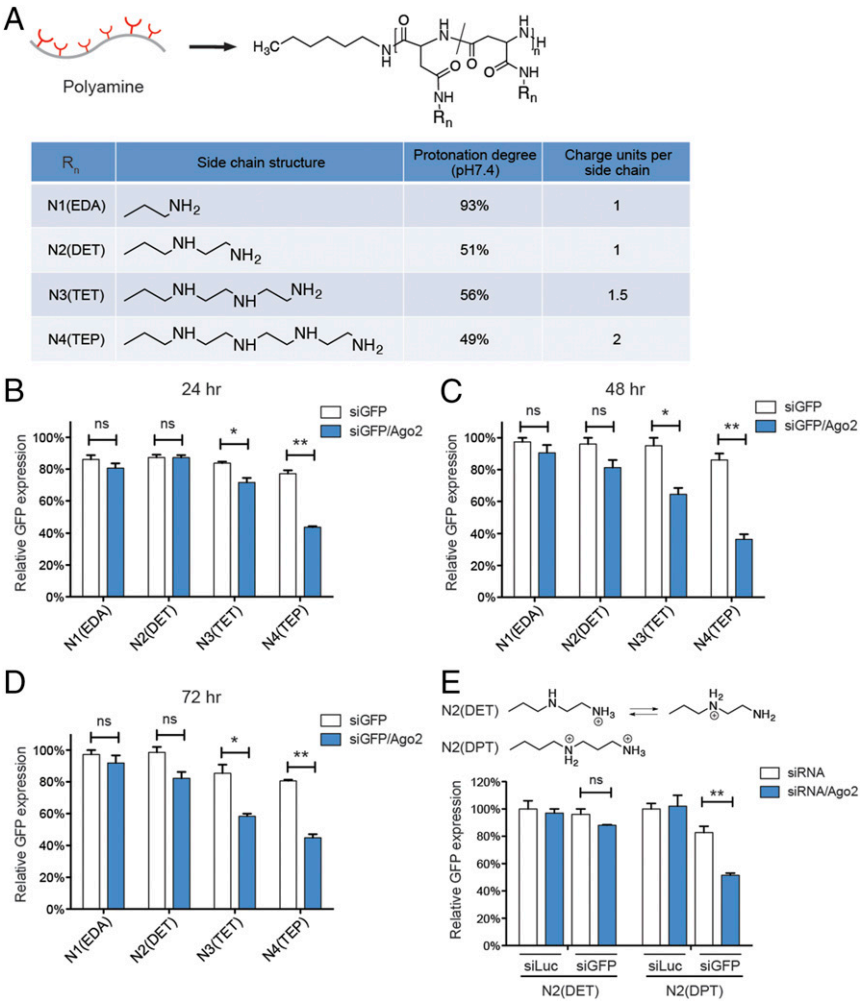

R_n	Side chain structure	Protonation degree (pH7.4)	Charge units per side chain
N1(EDA)	NH_2	93%	1
N2(DET)	NH NH_2	51%	1
N3(TET)	NH NH NH_2	56%	1.5
N4(TEP)	NH NH NH NH_2	49%	2

Fig. 3. siRNA/Ago2 complexed with polyamines induces structure-dependent gene silencing. (*A*) Structures and charge properties of polyamines utilized in the study. Note that the amination of the backbone induces an intramolecular isomerization of the repeating unit, aspartamide, generating two isomers (43). Charge units on each side chain are estimated by taking into account the numbers of primary and secondary amines and the protonation degree at pH 7.4, 150 mM NaCl, 37 °C, which was determined by a potentiometric titration. (*B–D*) Codelivery of 100 nM ds siGFP/Ago2 resulted in enhanced GFP silencing in 293Td2GFP cells compared with siGFP alone in a polyamine side-chain–dependent manner. GFP expression was quantified via flow cytometer at (*B*) 24, (*C*) 48, and (*D*) 72 h after transfection, and was normalized to that of nontransfected 293Td2GFP cells. (*E*) Increased side-chain protonation from N2(DET) to N2(DPT) augments GFP knockdown with siGFP and Ago2. The estimated protonated structures of N2(DET) and N2(DPT) at pH 7.4 are shown at the top. ss siLuc and ds siLuc was used as a nontargeting control. Mean fluorescence intensity of GFP expression was quantified via flow cytometry and normalized to that of 293Td2GFP cells. Data are represented as the mean ± SEM ($n = 3$). *$P < 0.05$, **$P < 0.01$, ns, no significance.

Therefore, N2 (DPT) improves gene silencing likely through increased electrostatic interactions with siRNA and Ago2.

Preassembly of siRNA/Ago2 Is Indispensable for Sustained Gene Silencing. Since Ago2 is considered the rate-limiting factor in the RNAi pathway, previous studies have exploited Ago2 overexpression in targeted cells to enhance gene silencing (31, 32). We thus asked whether the physical preclustering of siRNA/Ago2 complex or the restoration of stoichiometric amounts of Ago2 within cells resulted in greater gene silencing in our study (Fig. 4*A*). To test the latter possibility, we genetically modified 293Td2GFP cells to stably overexpress Ago2 using lentivirus. siGFP was subsequently transfected into these cells via each of the four different polyamines. At 24-h posttransfection, GFP expression was reduced in Ago2-overexpressing cells, with all four polyamines. In addition, during the first 24 h, the degree of GFP silencing with Ago2 overexpression was higher than that with siGFP/Ago2 complexes in 293Td2GFP cells for N1(EDA), N2(DET), and N3(TET) (Fig. 4*B*). This trend reversed at longer times, and at 48- and 72-h posttransfection, codelivering siGFP/Ago2 complexes outcompeted Ago2 overexpression in downregulating GFP levels via N3 (TET) and N4 (TEP) (Fig. 4 *C* and *D*). On the contrary, siRNA against luciferase (siLuc) failed to silence GFP expression through codelivery of Ago2 protein or in the presence of Ago2 overexpression, suggesting sequence-specific knockdown by siGFP/Ago2 with different polyamines (*SI Appendix*, Fig. S5).

To rule out the possibility that overexpressing Ago2 via the lentiviral system may not have increased Ago2 to the same levels as direct delivery of Ago2 protein, we monitored the total Ago2 levels in cells upon delivery of preassembled siRNA/Ago2 (1:1 molar ratio) packaged with N4 (TEP) over 72 h by Western blotting. The amount of Ago2 protein added into culture medium relative to the cell number in Western blotting assays remained the same as in the in vitro transfection studies as shown in Fig. 3. Unexpectedly, the amount of Ago2 introduced into cells through delivery of siRNA/Ago2 complexes was nearly undetectable compared with in cells transfected with siRNA

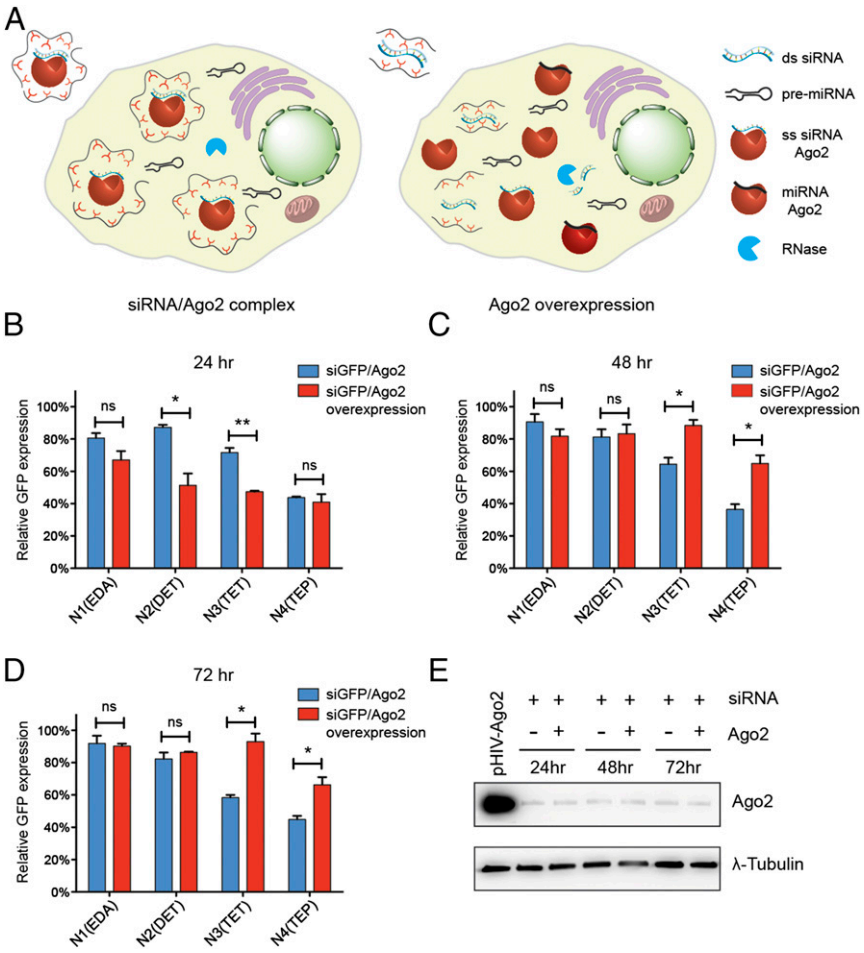

Fig. 4. Preassembly of the siRNA/Ago2 complex is indispensable for sustained gene silencing. (*A*) Two different siRNA delivery schemes. Physical coassembly of duplex siRNA and Ago2 may promote intracellular formation of RISC comprising ss antisense RNA and Ago2 (*Left*), whereas transfection of siRNA into cells overexpressing Ago2 does not facilitate loading of siRNA to Ago2 due to potential competition with endogenous miRNA species or RNA degradation (*Right*). (*B*) Stable overexpression of Ago2 in 293Td2GFP transiently resulted in lower GFP expression 24 h after transfection of 100 nM siGFP, compared with transfection of 100 nM siGFP/Ago2 in 293Td2GFP cells. At (*C*) 48 and (*D*) 72 h after transfection, however, siGFP/Ago2 complexes demonstrated greater GFP silencing than siGFP alone in 293Td2GFP cells overexpressing Ago2 via N3(TET) and N4(TEP). Data are represented as the mean ± SEM ($n = 3$). *$P < 0.05$, ns, no significance. (*E*) Western blotting of total Ago2 levels from cells transduced with lentivirus pHIV-Ago2, transfected with siRNA alone or siRNA/Ago2 protein via N4(TEP) polyamine for different hours (24, 48, and 72 h). While delivery of siRNA/Ago2 protein did not raise Ago2 level relative to siRNA-transfected cells, genetic overexpression substantially increased Ago2 level.

alone. Moreover, the Ago2 level in cells stably overexpressing this gene far exceeded that of basal Ago2 expression in siRNA/Ago2-transfected cells (Fig. 4*E*). Therefore, simply raising the level of Ago2 inside cells does not explain the improved gene silencing achieved via preassembly of siRNA/Ago2. Furthermore, codelivery of siRNA and Ago2 protein is likely a prerequisite for enhancement of siRNA-mediated gene silencing. We hypothesized that strong electrostatic interactions between the positively charged polypeptide used as a carrier and the negatively charged siRNA/Ago2 complexes lead to nanoplexed structures that keep the nucleic acid and protein stably bound for extended periods, thus improving the trafficking of siRNA in a prebound form for gene silencing (Fig. 4*A*).

The Side Chains of Polyamines Modulate Nanoscale Distances That Define Functional Assembly of siRNA and Ago2. Endogenous small RNA species such as miRNAs are abundant inside cells and can potentially compete with delivered siRNA for cotransfected Ago2 proteins (13). Therefore, we reasoned that physical stabilization of the siRNA preassembly with Ago2 when packaged in the nanocomplexes is critical for maintaining the assembled system during intracellular trafficking ultimately to the target mRNA. To address whether polyamines differentially modulate the physical interactions between siRNA and Ago2 inside nanocomplexes, siRNA and Ago2 protein were labeled with fluorescein isothiocyanate (FITC) and cyanine 5 (Cy5), respectively. In principle, when these two dyes are in close vicinity to each other (<10 nm), Förster resonance energy transfer (FRET) can be detected by flow cytometry. Consequently, an intracellular FRET assay is able to quantitatively evaluate the proximity between Ago2 and siRNA following cotransfection into an intracellular environment (Fig. 5*A*). By longitudinally measuring mean FRET intensity, it was found that the number of charged amine groups on the side chain is proportional to the degree of colocalization between FITC-siRNA and Cy5-Ago2 over the course of 72 h after transfection of 293T cells (Fig. 5 *B* and *C*). Interestingly, this observation correlated with the ability of the polyamines to enhance siRNA-mediated GFP silencing and to maintain it for extended periods (Fig. 3 *B*–*D*). Therefore, our results suggest that in addition to facilitating cellular uptake, polyamines with distinct side-chain structures also serve to impact the assembly and activity

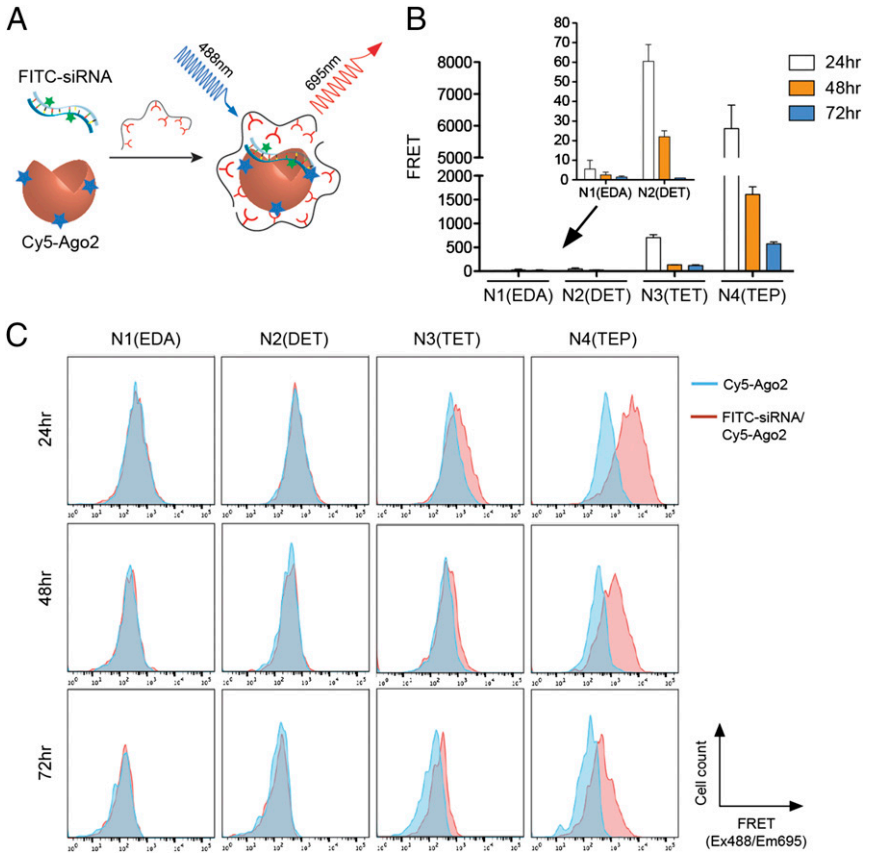

Fig. 5. The polyamine side-chain structure stabilizes nanoscale interactions between siRNA and Ago2. (*A*) A schematic of investigating polyamine-stabilized siRNA/Ago2 complex formation by FRET. (*B*) Mean FRET intensity to measure the degree of colocalization between FITC-siRNA and Cy5-Ago2. At 24, 48, and 72 h after transfection of Cy5-Ago2 or FITC-siRNA/Cy5-Ago2 into HEK293T cells with each polyamine, cells were analyzed by flow cytometry with a 488-nm laser and 695-nm detector with a 40-nm bandwidth. FRET values were calculated by subtracting the fluorescence signal of Cy5-Ago2-transfected cells from that of FITC-siRNA/Cy5-Ago2-transfected cells. Data are represented as the mean ± SEM ($n = 3$). (*C*) Representative histograms of intracellular FRET assays at 24-, 48-, and 72-h posttransfection.

of siRNA/Ago2, which is critical for Ago2-mediated enhancement of gene silencing.

The mRNA Cleavage Activity of Ago2 Is Primarily Responsible for Enhanced Gene Silencing. Among the four Ago members in mammalian cells, only Ago2 is able to cleave target mRNA (33). To test whether its intrinsic endonuclease activity was required for enhancing siRNA-mediated knockdown, we generated a catalytically inactive mutant, Ago2(D669A) (*SI Appendix*, Fig. S9*A*) (34). It was found that the slicing deficiency fully abolished the enhancement of siGFP-mediated silencing using N1 (EDA), N2 (DET), and N3 (TET) (*SI Appendix*, Fig. S9*B*). Interestingly, with N4 (TEP), the mutant Ago2 protein slightly increased siGFP-mediated silencing in comparison with siGFP alone but to a much lower degree than the wild-type Ago2 (*SI Appendix*, Fig. S9*B*). According to previous work, the endonuclease-inactive Ago2(D669A) protein remains able to bind ds siRNA and repress mRNA translation through the miRNA pathway (34, 35). Therefore, given the fact that N4 (TEP) induced the strongest clustering of siRNA/Ago2 in the cytoplasm based on our FRET studies, we reasoned that Ago2(D669A)/N4 (TEP) likely represses mRNA translation despite lower gene-silencing efficiency compared with direct mRNA cleavage.

Preassembly of Ago2 with siRNA Against Oncogenes in Melanoma Cells. Having confirmed the silencing potency of siRNA/Ago2 with GFP, we chose a therapeutic target, STAT3, as its overexpression has been associated with malignancy (23, 24). We first utilized an experimentally validated anti-STAT3 siRNA (siSTAT3) sequence from published studies (36, 37), and confirmed cytosolic colocalization of FITC-siSTAT3 and Cy5-Ago2 in B16F10 cells at 24 h after N4 (TEP)-mediated transfection (Fig. 6*A*). Additionally, the majority of siRNA/Ago2 nanoplexes escaped from late endosomes and lysosomes, as evidenced by imaging Cy5-labeled Ago2 and immune staining against Rab7, a marker for late endocytosis, at 24-h posttransfection with N4 (TEP) (*SI Appendix*, Fig. S10). Next, siSTAT3 was transfected alone or codelivered with Ago2 via N4 (TEP) into B16F10 cells. Enhanced STAT3 knockdown through siSTAT3/Ago2 was observed at both the mRNA and protein levels (Fig. 6 *B* and *C*). In addition to enhanced target gene knockdown, we asked whether this could translate into cancer inhibition. A single transfection of siSTAT3 along with Ago2 and N4 (TEP) induced pronounced growth inhibition of melanoma cells for up to 5 d, whereas siSTAT3 with N4 (TEP) failed to do so (Fig. 6*D*). Such an observation can be corroborated by an earlier study that reported a half-life of greater than 5 d for Ago2 (38). Additionally, we speculated that such an increased proliferation inhibition resulted from a more stabilized siRNA/Ago2 complex through N4 (TEP) in the cytoplasm of B16F10 cells, which was demonstrated in the aforementioned GFP silencing and FRET studies (Figs. 3 *B–D* and 5).

Delivery of siSTAT3/Ago2 Reduces Tumor Burden and Increases Survival in a Melanoma Mouse Model. Having confirmed the in vitro efficacy of siSTAT3/Ago2 with N4 (TEP), we investigated

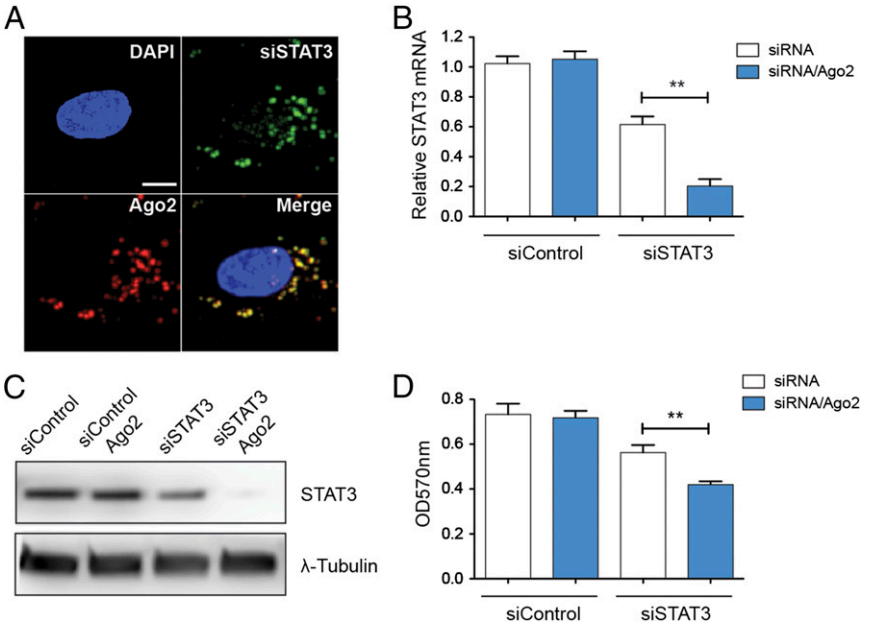

Fig. 6. Cytosolic delivery of siSTAT3/Ago2 inhibits proliferation of melanoma cells in vitro. (*A*) Colocalization of siSTAT3 and Ago2 in B16F10 cells. FITC-siSTAT3 (100 nM)/Cy5-Ago2 (1:1 molar ratio) were transfected into B16F10 cells via N4(TEP). At 24-h posttransfection, cells were imaged with confocal microscopy. Nuclei were stained with DAPI. (Scale bar: 10 μm.) For in vitro silencing of STAT3, B16F10 cells were transfected with 100 nM siRNA/Ago2 or siRNA alone for 48 h. siSTAT3/Ago2 significantly enhanced gene silencing over siSTAT3 alone detected at the (*B*) mRNA and (*C*) protein levels. siControl represents an siRNA with a scrambled sequence. (*D*) siSTAT3/Ago2 reduced cell proliferation in comparison with siSTAT3 at 120 h after a single transfection. Cell proliferation was measured by an MTT assay. Data are represented as the mean ± SEM ($n = 3$). $^{**}P < 0.01$.

the synergistic preassembly in a well-established mouse melanoma model. C57BL/6 mice were challenged with B16-F10 tumor cells on day 0 and, after primary tumor establishment, N4 (TEP)-packaged siSTAT3 and siSTAT3/Ago2 (along with corresponding control siRNA) were injected at 5 μg siRNA per tumor on days 7, 10, 13, and 16 (Fig. 7*A*). The tumor size was measured every 3 d and used as an indication of cancer progression. Treatment with siSTAT3/Ago2 significantly reduced tumor burden and prolonged animal survival relative to control groups (Fig. 7 *B* and *C*). To understand the underlying mechanisms, we administered the same treatment four times to separate batches of mice. Two days after the last treatment, tumor-derived samples were stained for STAT3 expression as well as with two markers for cell proliferation (Ki67 positive) and apoptosis (active caspase 3 positive). Consistent with the tumor measurements and survival study, only siSTAT3/Ago2-treated tumors resulted in reduced STAT3 expression (Fig. 7*D*). In addition, the inhibitory effect of siSTAT3/Ago2 on tumor progression was attributed to decreased cell proliferation, as evidenced by much fewer Ki67-positive nuclei (Fig. 7*D*). In contrast, the staining for cleaved caspase 3, a hallmark of apoptotic cells, showed that delivery of siSTAT3/Ago2 did not appreciably induce cell apoptosis, with a lack of noticeable differences across different treatment regimes (Fig. 7*D*). Therefore, we conclude that preassembly of siSTAT3 and Ago2 can potentially exert great therapeutic efficacy by inhibiting cancer cell proliferation.

Discussion

In this work, we investigated fundamental structure–activity relationships for the optimal assembly and silencing efficacy of siRNA/Ago2, by exploring structurally defined polyamines as delivery vehicles. We showed that the functional clustering of siRNA/Ago2 is dependent on the polyamine side-chain structure, which directly impacts the degree of gene silencing. This demonstrates that the gene delivery vehicle itself can also modulate RNAi machinery activity, in addition to other mechanisms that have been previously exploited for enhanced gene silencing, such as the improvement of siRNA stability, uptake, and endosomal escape. As a result, our study suggests that characterization of the dynamic interactions between the synthetic delivery vehicle, siRNA, and the complementary proteins responsible for RNAi can provide a unique avenue toward the development of new vehicles with significantly greater therapeutic efficacy. Earlier studies have investigated modification of polyethyleneimine with fatty acids and targeted delivery of anti-STAT3 siRNA to improve the therapeutic efficacy of silencing STAT3 expression in the B16F10 melanoma model, respectively, and these approaches induced similar levels of tumor suppression compared with our system (36, 39). To further enhance the magnitude of gene silencing via codelivery of siRNA/Ago2, future studies can incorporate hydrophobic and targeting moieties into existing polyamines. Alternatively, screening other delivery platforms (e.g., liposomes and lipoplexes) can identify new carriers to maximize the therapeutic index of siRNA/Ago2 complexes for clinical translation.

In addition, we found that preassembling ds siRNA with the Ago2 protein elicited much more potent gene silencing than a single-guide strand-loaded Ago2 when transfecting mammalian cells. The latter format is known to be the minimal RISC, which comprises a 5′-phosphorylated ss RNA and Ago2, and has recently been utilized to transfect RNAi-deficient parasites for fundamental studies on host–parasite interactions via a commercial transfection reagent (17). We reasoned that the preassembly of ds siRNA with Ago2 may help recruit several other intracellular components such as dicer and transactivation response RNA-binding protein, which are known to facilitate siRNA loading (15). Nevertheless, several experimental observations show that Ago2 itself can process ds siRNA into a single-guide RNA, which subsequently forms an RISC complex to cleave target mRNA in vitro (15, 16, 40). Future work can investigate whether ds siRNA alone or in concert with intracellular

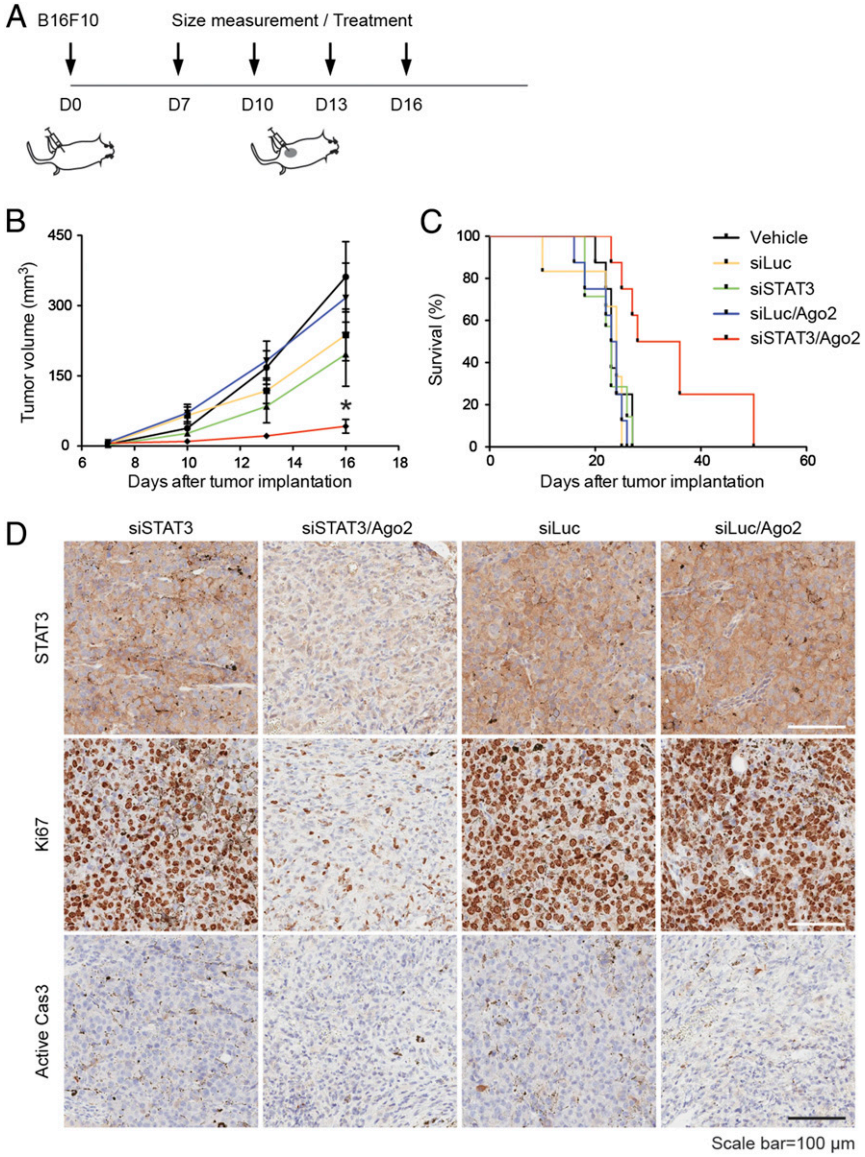

Fig. 7. Therapeutic efficacy of siSTAT3/Ago2 in melanoma model. (*A*) Schedule of tumor inoculation and therapeutic treatment. B16F10 cells (0.5 million) were implanted s.c. in C57BL/6 mice. Mice received intratumoral injections of nanoplexes containing 5 μg siRNA against luciferase (siLuc), siSTAT3, or siRNA with equimolar amounts of Ago2, which were packaged with N4(TEP) at a 20:1 N/P ratio. (*B*) Tumor size measurements were taken every 3 d before each injection on the same day and discontinued when some mice in the control groups were euthanized due to large tumor burden. (*C*) Kaplan–Meier survival curve for different treatment regimes. siSTAT3/Ago2 significantly extended the survival of B16F10-challenged mice. Vehicle control, siLuc/Ago2, and siSTAT3 ($n = 7$); siLuc ($n = 6$), and siSTAT3/Ago2 ($n = 8$). *$P < 0.05$. (*D*) Expression of STAT3, K_i-67 (cell proliferation marker), and active caspase 3 (apoptotic marker) in tumor samples detected by immunohistological staining 48 h after the last administration of four treatments in a separate study.

components enables RISC assembly and activation in our preassembly system. In addition, we observed that the physical clustering of siRNA/Ago2 was critical for sustained gene silencing. On the contrary, overexpression of Ago2 before siRNA transfection was found to be less efficient and less sustained over time. Our findings can be corroborated by a fundamental study showing that the abundance of Ago2-bound siRNA determines RNAi efficacy in vivo (12). As a result, our coassembly system utilizing strong interactions between polyamines and preassembled siRNA/Ago2 complexes can potentially be exploited to silence multiple mRNA targets to different degrees by tuning the stoichiometry of different siRNA/Ago2 complexes as well as by selecting different polyamines for delivery. This strategy may provide a toolset for systems and synthetic biology, which require simultaneous perturbation of multiple genes for analyses of complex biological networks. In addition, targeting different mRNAs can be effective for treating diseases such as cancer that are often driven by multiple genetic mutations.

Materials and Methods

Chemicals and Antibodies. All chemicals, cell lines, antibodies, and mice are provided in *SI Appendix, Materials and Methods*. All reagents are available to share with the public.

Synthesis and Characterization of Polyamines. Polyamines were synthesized according to a modified procedure of Uchida et al. (18). Briefly, to a chilled solution of PBLD in *N*-Methyl-2-pyrrolidone (NMP) (2 mL), 50 equivalents of polyamine diluted twofold with NMP was added dropwise with stirring. After stirring for 2 h at 0 °C, the pH was adjusted to 1 with dropwise addition while stirring of cold 6 M HCl. The resulting solution was dialyzed from a regenerated cellulose membrane bag (1 kDa MWCO; Spectrum Laboratories)

against 0.01 M HCl followed by mQ water, frozen, and lyophilized to give a white powder.

Production and Purification of Recombinant Human Ago2. RNA-free hAgo2 was expressed and purified as previously described (13). Briefly, 10 L of *SF9* insect cells were infected with baculovirus-expressing Strep-sumo-hAgo2 for 72 h. Initial purification using Strep-Tactin resin (IBA Life Sciences) was followed by tag removal with TEV protease. RNA-free hAgo2 was separated from the endogenous RNA-loaded hAgo2 using a Mono S column and further purified on a superdex 200 increase column concentrated to 0.5 mg/mL and stored at −80 °C in 50 mM Tris, 100 mM KCl, and 10% glycerol.

Dynamic Light-Scattering Measurements of Nanoplexes. siRNA (5 μg) or siRNA (5 μg)/Ago2 (1:1 siRNA:Ago2 molar ratio) complexes were mixed with each polyamine at a 20:1 (N/P) ratio in a 50 μL assembly buffer (20 mM Hepes, 150 mM KCl, 2 mM $MgCl_2$, pH 7.4) for 30 min, and then were diluted to 1 mL with 20 mM Hepes as previously described (41). Final siRNA concentration in dynamic light-scattering (DLS) measurements was 5 μg/mL Hydrodynamic size was measured using DLS (Malvern ZS90 particle analyzer, $\lambda = 633$ nm). Zeta-potential measurements were made using laser Doppler electrophoresis with the Malvern ZS90.

Preparation of Nanoplexes for Transfection. Polyamines were dissolved in 10 mM Hepes buffer (pH 7.4) and adjusted to 10 mg/mL. For each well of a 96-well plate, siRNA diluted in 5 μL assembly buffer (20 mM Hepes, 150 mM KCl, 2 mM $MgCl_2$, pH 7.4) was mixed with 5 μL assembly buffer containing recombinant Ago2 at the desired molar ratio at room temperature for 30 min. Afterward, polyamine diluted in 5 μL assembly buffer was added and incubated at room temperature for 15 min before transfection. Polyamine was adjusted to obtain a 20:1 N/P ratio for transfection studies.

Quantitative PCR. Forty-eight hours after transfection, total RNA was extracted by an RNeasy Plus Mini kit (Qiagen) and converted to cDNA with an Ecodry cDNA synthesis kit (Clontech). cDNA was amplified with a LightCycler 480 SYBR Green I Master reagent and quantified by a Roche LightCycler 480 Real-Time PCR System. Primer sequences used for detection are available in *SI Appendix*. A common $2^{-\Delta\Delta CT}$ method was applied to data with automatic removal of background fluorescence by the qPCR-associated software. qPCR primers used in this study are provided below.

Western Blot. Cells were lysed in a lysis buffer (20 mM Tris pH 7.5, 150 mM NaCl, 1% Nonidet P-40, 0.5% Sodium Deoxycholate, 1 mM EDTA, 0.1% SDS, protease inhibitors). Proteins were first separated by 4–15% SDS/PAGE and then transferred to a nitrocellulose membrane (ThermoFisher). The membranes were incubated with primary antibodies: anti-tubulin (clone G-8, 1:1,000; Santa Cruz), anti-STAT3 (clone 124H6, 1:2,000; Cell Signaling), and anti-c-MET (clone D1C2, 1:2,000; Cell signaling) in 5% milk/TBS buffer (25 mM Tris pH 7.4, 150 mM NaCl, 2.5 mM KCl) at 4 °C overnight, and then probed for 1 h with secondary horseradish peroxidase-conjugated anti-mouse or anti-rabbit IgG (Santa Cruz).

Intracellular FRET. Ago2 protein was labeled with Cy5-NHS (AAT bioquest) at a 5:1 (dye/protein) molar ratio directly in the protein storage buffer (50 mM Tris, 100 mM KCl, and 10% glycerol) at room temperature for 1 h. On the day of transfection, FITC-siRNA (100 nM final concentration) alone or 100 nM FITC-mRNA/Cy5-Ago2 (1:1 siRNA:Ago2 molar ratio) were transfected with polyamines at N/P 20 into cells. Cells were harvested at 24-, 48-, and 72-h posttransfection. Fluorescence intensity of the cells was monitored and evaluated with an FACSCelesta (BD Biosciences) equipped with Diva software (BD Biosciences), using a 488 laser for excitation and a 695/40-nm filter.

Immunocytochemistry. Transfection and immune staining were performed in Millicell EZ chamber slides (Milliporesigma). Cells were fixed by 4% formaldehyde in PBS for 15 min, permeabilized by 0.4% Triton X-100 on ice for 10 min, and stained with a rabbit anti-Rab7 antibody (1:400, #9367; Cell signaling) overnight at 4 °C. After washing with PBS containing 0.05% Tween-20, cells were stained with an Alexa 568-conjugated goat anti-rabbit antibody (4 μg/mL, #A-11011; ThermoFisher). Nuclei were counterstained with DAPI. Cells were imaged with an Inverted Olympus IX83 microscope equipped with a Hamamatsu ImagEM high-sensitivity camera at the Swanson Biotechnology Center, Massachusetts Institute of Technology (MIT).

Animal Experiments. Mouse care and experimental procedures were performed under pathogen-free conditions in accordance with established institutional guidelines and approved protocols from the MIT Division of Comparative Medicine. For s.c. tumor challenge, we injected 0.5 million B16F10 cells (American Type Culture Collection) into 7–8-wk-old C57BL/6. After tumors reached an average size of ∼3 mm (day 7 posttumor inoculation), mice were injected intratumorally four times every 3 d with nanocomplexes containing 5 μg siRNA against luciferase (negative control), siSTAT3 or siRNA with an equimolar amount of Ago2. Tumor volume was calculated using $V = (L \times W \times W)/2$, where V is tumor volume, W is tumor width, and L is tumor length. Survival studies were completed when the last mouse was euthanized, and a Kaplan–Meier survival curve was plotted to evaluate the efficacies of different treatments.

Immunohistochemistry Staining. Tumor samples were obtained at 48 h following the last treatment in C57BL/6 mice. Tumors were formalin-fixed for 24 h and paraffin-embedded afterward. All formalin-fixed paraffin-embedded slides were antigen retrieved using heat-induced epitope retrieval at 97 °C for 20 min using citrate buffer (pH 6). An automated machine (IHC Autostainer 360; ThermoScientific) run consisted of endogenous peroxidase blocking (10 min), protein block (30 min), primary antibody (60 min), labeled polymer (15 min), and 3,3′-Diaminobenzidine (DAB) (10 min). The entire IHC was processed by the Swanson Biotechnology Center (MIT).

Statistical Analysis. All statistical analyses were performed using GraphPad Prism 5.0a for Mac OS X. A one-way ANOVA followed by a Tukey posttest or Student's *t* test was used to determine statistical significance in the studies.

ACKNOWLEDGMENTS. We thank Glenn Paradis at the David H. Koch Institute Flow Cytometry Core at MIT for providing assistance in the intracellular FRET experiment; and the Department of Comparative Medicine at MIT for assistance with animal study. This work was supported by the Department of Defense (DoD) Ovarian Cancer Research Program Teal Innovator Award (to P.T.H.), the DoD Peer Reviewed Orthopaedic Research Program Idea Development Award (to P.T.H.), and the Koch Institute Quinquennial Postdoctoral Fellowship (to J.L.). C.W. acknowledges the National Science Foundation Graduate Research Fellowship. L.J.-T. is an investigator of the Howard Hughes Medical Institute.

1. Wittrup A, Lieberman J (2015) Knocking down disease: A progress report on siRNA therapeutics. *Nat Rev Genet* 16:543–552.
2. Leuschner F, et al. (2011) Therapeutic siRNA silencing in inflammatory monocytes in mice. *Nat Biotechnol* 29:1005–1010.
3. Schaefer KA, et al. (2017) Unexpected mutations after CRISPR-Cas9 editing in vivo. *Nat Methods* 14:547–548.
4. Dai WJ, et al. (2016) CRISPR-Cas9 for in vivo gene therapy: Promise and hurdles. *Mol Ther Nucleic Acids* 5:e349.
5. Xue HY, et al. (2016) In vivo gene therapy potentials of CRISPR-Cas9. *Gene Ther* 23: 557–559.
6. Kanasty R, Dorkin JR, Vegas A, Anderson D (2013) Delivery materials for siRNA therapeutics. *Nat Mater* 12:967–977.
7. Corey DR (2007) Chemical modification: The key to clinical application of RNA interference? *J Clin Invest* 117:3615–3622.
8. Mok H, Lee SH, Park JW, Park TG (2010) Multimeric small interfering ribonucleic acid for highly efficient sequence-specific gene silencing. *Nat Mater* 9:272–278.
9. Lee JB, Hong J, Bonner DK, Poon Z, Hammond PT (2012) Self-assembled RNA interference microsponges for efficient siRNA delivery. *Nat Mater* 11:316–322.
10. Laffont B, et al. (2013) Activated platelets can deliver mRNA regulatory Ago2•microRNA complexes to endothelial cells via microparticles. *Blood* 122:253–261.
11. Lv Z, et al. (2014) Argonaute 2 in cell-secreted microvesicles guides the function of secreted miRNAs in recipient cells. *PLoS One* 9:e103599.
12. Wei J, et al. (2011) RNA-induced silencing complex-bound small interfering RNA is a determinant of RNA interference-mediated gene silencing in mice. *Mol Pharmacol* 79: 953–963.
13. Elkayam E, et al. (2012) The structure of human argonaute-2 in complex with miR-20a. *Cell* 150:100–110.
14. Rivas FV, et al. (2005) Purified argonaute2 and an siRNA form recombinant human RISC. *Nat Struct Mol Biol* 12:340–349.
15. Noland CL, Doudna JA (2013) Multiple sensors ensure guide strand selection in human RNAi pathways. *RNA* 19:639–648.
16. Deerberg A, Willkomm S, Restle T (2013) Minimal mechanistic model of siRNA-dependent target RNA slicing by recombinant human argonaute 2 protein. *Proc Natl Acad Sci USA* 110:17850–17855.
17. Castellanos-Gonzalez A, Perry N, Nava S, White AC, Jr (2016) Preassembled single-stranded RNA-argonaute complexes: A novel method to silence genes in cryptosporidium. *J Infect Dis* 213:1307–1314.
18. Uchida H, et al. (2014) Modulated protonation of side chain aminoethylene repeats in N-substituted polyaspartamides promotes mRNA transfection. *J Am Chem Soc* 136: 12396–12405.

19. Itaka K, Ishii T, Hasegawa Y, Kataoka K (2010) Biodegradable polyamino acid-based polycations as safe and effective gene carrier minimizing cumulative toxicity. *Biomaterials* 31:3707–3714.
20. Aini H, et al. (2016) Messenger RNA delivery of a cartilage-anabolic transcription factor as a disease-modifying strategy for osteoarthritis treatment. *Sci Rep* 6:18743.
21. Uchida H, et al. (2011) Odd-even effect of repeating aminoethylene units in the side chain of N-substituted polyaspartamides on gene transfection profiles. *J Am Chem Soc* 133:15524–15532.
22. Li Y, et al. (2015) Suppression of cancer relapse and metastasis by inhibiting cancer stemness. *Proc Natl Acad Sci USA* 112:1839–1844.
23. Yu H, Pardoll D, Jove R (2009) STATs in cancer inflammation and immunity: A leading role for STAT3. *Nat Rev Cancer* 9:798–809.
24. Pan Y, et al. (2017) Stat3 contributes to cancer progression by regulating Jab1/Csn5 expression. *Oncogene* 36:1069–1079.
25. Bu P, et al. (2013) A microRNA miR-34a-regulated bimodal switch targets Notch in colon cancer stem cells. *Cell Stem Cell* 12:602–615.
26. Raemdonck K, et al. (2006) In situ analysis of single-stranded and duplex siRNA integrity in living cells. *Biochemistry* 45:10614–10623.
27. Lin CY, et al. (2016) Messenger RNA-based therapeutics for brain diseases: An animal study for augmenting clearance of beta-amyloid by intracerebral administration of neprilysin mRNA loaded in polyplex nanomicelles. *J Control Release* 235:268–275.
28. Li J, et al. (2017) Structurally programmed assembly of translation initiation nanoplex for superior mRNA delivery. *ACS Nano* 11:2531–2544.
29. Li J, et al. (2017) Polyamine-mediated stoichiometric assembly of ribonucleoproteins for enhanced mRNA delivery. *Angew Chem Int Ed Engl* 56:13709–13712.
30. Miyata K, et al. (2008) Polyplexes from poly(aspartamide) bearing 1,2-diaminoethane side chains induce pH-selective, endosomal membrane destabilization with amplified transfection and negligible cytotoxicity. *J Am Chem Soc* 130:16287–16294.
31. Diederichs S, et al. (2008) Coexpression of argonaute-2 enhances RNA interference toward perfect match binding sites. *Proc Natl Acad Sci USA* 105:9284–9289.
32. Börner K, et al. (2013) Robust RNAi enhancement via human argonaute-2 overexpression from plasmids, viral vectors and cell lines. *Nucleic Acids Res* 41:e199.
33. Wang B, et al. (2009) Distinct passenger strand and mRNA cleavage activities of human argonaute proteins. *Nat Struct Mol Biol* 16:1259–1266.
34. Tan GS, et al. (2009) Expanded RNA-binding activities of mammalian argonaute 2. *Nucleic Acids Res* 37:7533–7545.
35. Liu J, et al. (2004) Argonaute2 is the catalytic engine of mammalian RNAi. *Science* 305:1437–1441.
36. Kortylewski M, et al. (2009) In vivo delivery of siRNA to immune cells by conjugation to a TLR9 agonist enhances antitumor immune responses. *Nat Biotechnol* 27:925–932.
37. Kortylewski M, et al. (2005) Inhibiting Stat3 signaling in the hematopoietic system elicits multicomponent antitumor immunity. *Nat Med* 11:1314–1321.
38. Olejniczak SH, La Rocca G, Gruber JJ, Thompson CB (2013) Long-lived microRNA-argonaute complexes in quiescent cells can be activated to regulate mitogenic responses. *Proc Natl Acad Sci USA* 110:157–162.
39. Alshamsan A, et al. (2010) The induction of tumor apoptosis in B16 melanoma following STAT3 siRNA delivery with a lipid-substituted polyethylenimine. *Biomaterials* 31:1420–1428.
40. Matranga C, Tomari Y, Shin C, Bartel DP, Zamore PD (2005) Passenger-strand cleavage facilitates assembly of siRNA into Ago2-containing RNAi enzyme complexes. *Cell* 123:607–620.
41. Troiber C, et al. (2013) Comparison of four different particle sizing methods for siRNA polyplex characterization. *Eur J Pharm Biopharm* 84:255–264.
42. Leuschner PJ, Ameres SL, Kueng S, Martinez J (2006) Cleavage of the siRNA passenger strand during RISC assembly in human cells. *EMBO Rep* 7:314–320.
43. Nakanishi M, Park JS, Jang WD, Oba M, Kataoka K (2007) Study of the quantitative aminolysis reaction of poly(beta-benzyl L-aspartate) (PBLA) as a platform polymer for functionality materials. *React Funct Polym* 67:1361–1372.